Available online at www.sciencedirect.com

ScienceDirect

Physics Procedia 12 (2011) 46–53

Physics Procedia

LiM 2011

Nanoparticle Generation During Laser Ablation and Laser-Induced Liquefaction

N. Haustrup*, G. M. O'Connor

National Centre for Laser Applications, School of Physics, National University of Ireland, Galway, Ireland

Abstract

Recently short-pulse laser sources have been investigated as a potential method for nanoparticle synthesis. Deposited aluminium, nickel and gold nanoparticles generated during nano- and femto-second laser ablation were analyzed using SEM and AFM. As the environment in which laser ablation takes place is known to influence the size of generated nanoparticles, a novel gas ambient that generates a transient liquid phase was investigated. This ambient offers favorable properties to overcome some issues typically encountered with ablation in gases or liquids alone. The Laser-Induced Liquefaction (LIL) process most notably lead to a reduced mean radius of aluminium nanoparticles from 36.8 nm in air to 12.7 nm.

Keywords: Metals; Laser ablation; Nanoparticles; Laser-Induced Liquefaction

1. Introduction

Computational (mostly molecular dynamic) simulations [1] and experimental investigations [2] have shown conclusively that short-pulse laser heating of solids results in nano-scale particles or droplets of the target material to be ejected. The details of the nanoparticle formation and evolution during this process, however, are still unclear and this lack of understanding has clear safety implications for all laser users. The interest in this process is not solely safety, as there is also opportunity to optimise the nanoparticle synthesis process and compete with current nanoparticle fabrication methods. The potential for producing pure nanoparticles without the introduction of stabilizing chemicals, is advantageous in a number of applications, particularly in the medical field. The key issue associated with nanoparticle generation during laser ablation is the control of nanoparticle size and distribution, as it is their size-dependent physical properties that ultimately make them so attractive. To control the nanoparticle size, it is first important to acquire a greater understanding of the process of nanoparticle generation and evolution during laser ablation.

This paper describes the results of an exploratory study into the different factors affecting the size of nanoparticles generated during laser ablation through probing the material, laser and ambient. The materials used

* Corresponding author. Tel.: +353 (91) 493595; Fax: +353 (91) 494594.
E-mail address: natalie.haustrup@nuigalway.ie.

1875-3892
doi:10.1016/j.phpro.2011.03.104

were three metals, aluminum, nickel and gold, which have varying influential properties of interest. Laser parameters, such as laser pulse duration and laser fluence were also investigated.

Finally the ambient effect was investigated by introducing the process of laser-induced liquefaction (LIL), which is a novel method of affecting the ambient conditions during nanoparticle generation. LIL is a process, in which, the ambient gas, tetrafluoroethane ($C_2H_2F_4$), decomposes during laser ablation of a target and forms a transient liquid by-product in the ablation site [3]. The transient liquid that forms exists in the ablation site for several seconds before evaporating. Previous studies have shown that the introduction of either heavy molecular weight gases [4] or liquids [5] during laser ablation strongly influence the final size distribution of nanoparticles. However, laser ablation in gases typically encounters problems of nanoparticle coagulation, leading to larger nanoparticles with a broader size distribution. Laser ablation in liquids equally finds problems due to cavitation bubbles or beam distortion [6]. Laser-Induced Liquefaction offers the potential of laser ablation in a dry ambient and the collection and transport of generated nanoparticles in a transient liquid ambient, thus reducing some of the problems encountered with nanoparticle generation in just a gas or a liquid [6].

2. Experimental

The key parts of the workstation included: the laser source and beam delivery system, the sample fixture, gas control/delivery and exhaust extraction. Laser ablation was carried out inside a simple polycarbonate enclosure, with an optical window in the lid. The enclosure had a gas inlet and outlet either side of a fixed stage under the optical window. Two lasers were used to compare nanoparticle generation with nanosecond and femtosecond pulse durations from three metals: aluminum (Al), nickel (Ni) and gold (Au). Each metal was laser ablated using either the Coherent AVIA 355-7000 nanosecond laser or the Amplitude Systems S-Pulse HP femtosecond laser. Both systems used a frequency-tripled diode pumped solid-state laser to generate a UV wavelength of 355 nm and 343 nm, respectively. The laser pulse energy used was at the pre-determined ablation threshold for each metal for each laser. The ablation threshold was determined as the minimum pulse energy required to ablate a hole of the dimensions of the laser beam. Each metal was placed on the stage within the gas enclosure under the optical window, through which the laser passes.

Two gases were compared, air and tetrafluoroethane ($C_2H_2F_4$, Air Products) at pressure adjusted flow rates. $C_2H_2F_4$ was selected due to its interesting behavior during UV laser ablation in which laser-induced liquefaction occurred. $C_2H_2F_4$ was regulated at 10 psi (0.68 atmospheric pressure) the volumetric flow meter indicator reading 1.6 L/min, calibrated volumetric flow rate Q_{C2H2F4} = 1.1 L/min and mass flow rate M_{C2H2F4} = 4.7 g/min. Trenches were also etched in flowing air with a dynamic configuration similar to the $C_2H_2F_4$ flow. The differential pressure was regulated to be 34 psi. The volumetric flow meter indicator was at 3.2 L/min; calibrated volumetric flow rate Q_{air} = 5.76 L/min; and mass flow rate M_{air}=5.76 g/min. The gas flowed across the metal surface prior to, during and after the laser ablation process. Five trenches of 5 mm length with a space of 0.5 mm between them were machined in the surface. The trenches were ablated with a single pass at 50 mm s^{-1} at their pre-determined ablation threshold fluence.

All characterization of the ablated particles was completed using Atomic Force Microscopy (AFM) and Scanning Electron Microscopy (SEM); these techniques provided complementary information. The ablated particles that re-deposited onto the surface of the metal following laser ablation were imaged and the particle height was determined from AFM images and the particle diameter from the SEM images. The Agilent 5500 Atomic Force Microscope was used and the technique applied was optimized for each sample but as the nanoparticles were only loosely adhered to the surface, care had to be taken not to drag the debris with the tip and distort the image. A soft cantilever (Arrow Silicon FMR-20, resonance frequency 75 kHz, force constant 2.8 N/m), tapping mode, scan speed 0.1 lines/s for a 1 μm^2 area. Low cantilever forces and high responsive feedback settings allowed for images of the nanoparticles to be acquired. The images were processed using PicoView 4.6 software. Particles were detected by setting a threshold height and over 500 particles were measured and averaged. The Carl Zeiss Ultra Plus SEM was used with a low

accelerating voltage of 1 keV, resolution was set to 1024 x 768, working distance of 5 mm and aperture size of 10 μm. Following acquisition, the image was set to binary and particles were distinguished from the background by manually setting the threshold range and the size of 500 particles were measured.

3. Results

Three metals, Al, Ni and Au were laser ablated at the pre-determined ablation threshold fluence under different conditions and the nanoparticles generated were measured using AFM and SEM. The first system measured the nanoparticle size and distribution generated during nanosecond laser ablation in flowing air. The SEM images in Figure 1 show that the material itself is highly influential on the eventual size of the nanoparticles produced. The mean radius and the standard deviation of the nanoparticles generated under these conditions increased from Au to Al to Ni from 10.4 ± 19.6 nm to 36.8 ± 29.0 nm and 53.7 ± 50.6 nm, respectively.

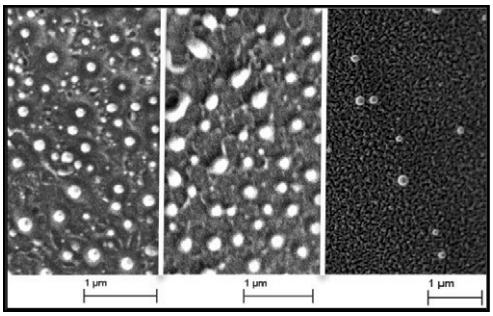

(a) (b) (c)

Figure 1. SEM images of the nanoparticles generated during nanosecond laser ablation in air of (a) Al, (b) Ni and (c) Au at their respective ablation threshold fluences.

The second system measured the nanoparticle size during femtosecond laser ablation in flowing air. The ablation threshold fluences for each material during femtosecond laser ablation were pre-determined for nanoparticle generation. The mean radius and standard deviation of the Au, Al and Ni nanoparticles generated under these conditions increased from 1.9 ± 1.2 nm to 9.1 ± 9.1 nm to 21.7 ± 33.9 nm, respectively. The difference between the nanoparticles formed following laser ablation with the nanosecond and femtosecond pulse duration is illustrated by the size distribution charts shown in Figure 2.

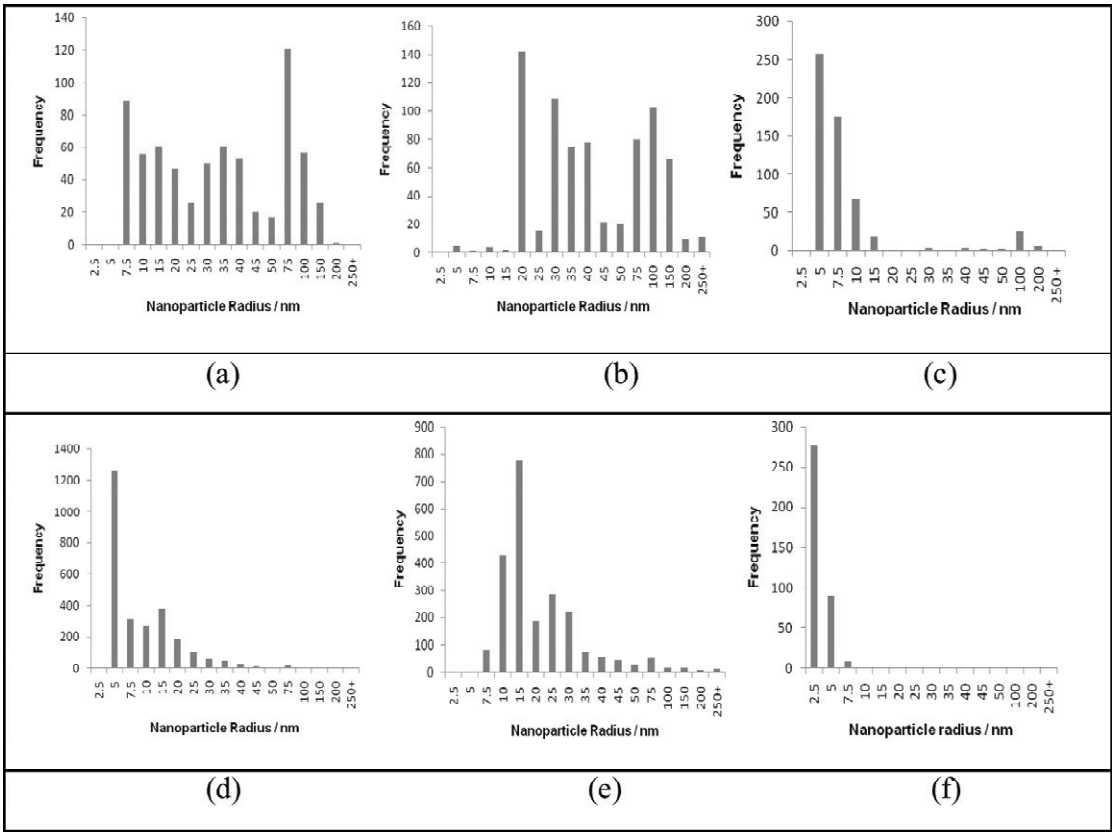

Figure 2. Comparison of the size distributions of nanoparticles produced during nanosecond laser ablation of (a) Al (b) Ni and (c) Au and femtosecond laser ablation of (d) Al (e) Ni and (f) Au. Data was acquired through analysis of SEM images.

Finally the influence of the ambient was probed by comparing nanoparticle generation in flowing air and in flowing $C_2H_2F_4$. The introduction of $C_2H_2F_4$ gas during nanosecond laser ablation resulted in a narrower size distribution of nanoparticles and a smaller mean size for all three metals. In particular, the radius of Al nanoparticles reduced from 36.8 ± 29.0 nm to 12.7 ± 12.3 nm with the standard deviation reduced by more than half relative to air. The size distribution of Ni and Au nanoparticles was also narrowed but some of the smallest nanoparticles generated in air were not present in $C_2H_2F_4$.. The distributions of nanoparticle radii generated during nanosecond laser ablation in $C_2H_2F_4$ from each metal are displayed in Figure 3.

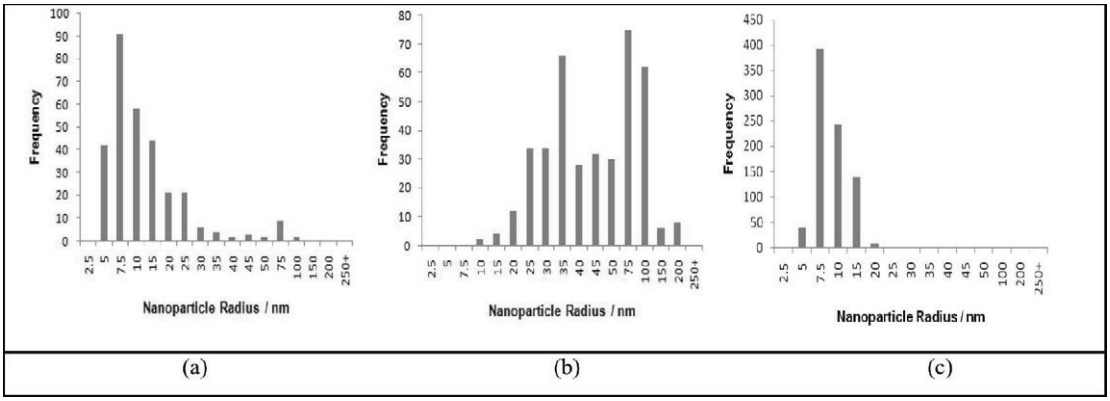

Figure 3. Size distribution of the radii of nanoparticles generated during nanosecond laser ablation in $C_2H_2F_4$ of (a) Al (b) Ni and (c) Au. Data was acquired through analysis of SEM images.

From all the results, it was shown that the material, laser and ambient all affect the nanoparticles size. Therefore it was considered that the optimum parameters for all these factors be applied to generate yet smaller nanoparticles. The results below show that by combining the optimum material, laser properties and ambient conditions it is possible to achieve smaller nanoparticles.

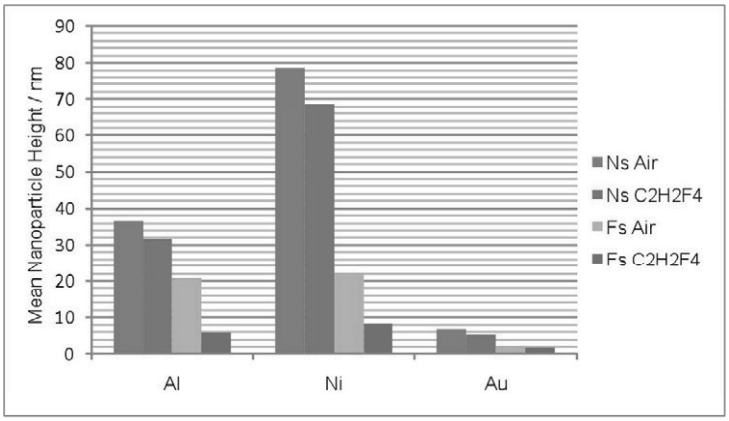

Figure 4. Comparison of the mean nanoparticle heights determined from AFM images. Conditions include nansecond laser ablation (Ns) in air, nanosecond laser ablation in $C_2H_2F_4$, femtosecond laser ablation (Fs) in air and femtosecond laser ablation in $C_2H_2F_4$ of the three metals

4. Discussion

The results showed that nanoparticle generation during laser ablation is a dynamic process and is governed by a number of factors. The laser-material-ambient interactions that occur during the laser ablation process, ejection of material and nanoparticle formation and evolution all influence the eventual size of the nanoparticles and the distribution. Laser pulse duration, fluence and beam shape were considered. Three materials with varying properties such as thermal conductivity, electron-phonon coupling time and surface energies were used. Finally the application of LIL to laser generation of nanoparticles was explored in comparison in ambient air.

The material response to the incident UV laser pulse is important and thus it was important to work at the ablation threshold of each material under each condition to keep the ablation mechanisms for each material comparable. The ablation threshold fluence relates to the minimum energy density (J/cm^2) absorbed by the material

to result in material ejection. This is therefore not only dependent on the laser pulse fluence, but also the material reflectivity and absorbance of the laser wavelength.

The difference in mean nanoparticle sizes observed for each material is attributed to several characteristic material properties including the electron-phonon coupling constant, thermal conductivity and surface energy, all of which affect different stages of the nanoparticle evolution. The process of laser ablation begins with the absorption of the laser pulse energy by the conduction band electrons of the target metal through the process of inverse Bremstrahlung. Following the heating of the electrons, the process of coupling this energy from the electrons to the lattice and is called electron-phonon coupling. The electron-phonon coupling constant, G_{ep}, determines the efficiency by which, the electrons, which have absorbed the incident laser photons couple with the vibrational modes of the lattice, thus transferring thermal energy. This then, in part, determines the volume of material that is heated and also the distribution of temperatures throughout that volume of material. If the material is uniformly heated, the material will undergo a uniform ablation mechanism and thus produce more uniform nanoparticles. Following ejection of nano-scale droplets the thermal conductivity of the material governs the time period, during which, the particles are in the molten form and therefore the period, during which, the nanoparticles have time to grow most efficiently. With Au having the highest electron-phonon coupling constant (22 x 10^{17} W m^{-3} K^{-1} at 25°C) and thermal conductivity (350 W m^{-1} K^{-1} at 25°C), it resulted in by far the smallest nanoparticles compared to e.g. Ni with an electron phonon coupling constant of 10.5 x 10^{17} W m^{-3} K^{-1} and a thermal conductivity 91 W m^{-1} K^{-1} [7, 8].

The surface energy of the material is also important; it governs the tendency of the particles to coagulate and thus result in a larger distribution of sizes. It is thermodynamically favorable for the nanoparticles to minimize the surface area exposed [9]. As Ni had the highest surface energy of the three metals studied, it was therefore more energetically favorable for the particles to exist with the smallest surface area exposed, resulting in fewer and larger particles as they coagulate. The surface energy of gold was the lowest of the metals studied and for this reason Au nanoparticles formed under a variety of conditions had a characteristically small size and distribution.

The laser properties were also shown to be highly influential on the nanoparticle size and distribution observed. The broad range of nanoparticles generated from each material under all conditions is attributed to the shape of the laser beam. The Gaussian beam shape incident on the material results in the volume of heated material with a non-uniform temperature distribution across the target material. As a result, nanoparticles of varying size and velocity profile are formed from different depths of the material.

It is clear from the results that the duration of the laser pulse incident on the material affects the eventual size of the nanoparticles. This can be explained through the laser-material interaction mechanisms, which differ greatly for shorter and longer pulse durations. This subsequently affects the volume of material heated, the efficiency of material heating and the ejection of material. In the nanosecond regime, the laser pulse is absorbed, electron-electron interactions and electron-phonon coupling all occur within the lifetime of the pulse. As these processes are occurring, the laser pulse incident on the target material continues to deliver more energy, which subsequently needs to be dispersed throughout the material. Electron-phonon coupling during the pulse transfers the thermal energy to the lattice and a large volume of material is heated. Additionally the temperature profile across the material and throughout the depth of the material varies greatly and this non-uniform distribution of heat leads to the ejection of material via different ablation mechanisms. The material that is ejected are therefore different sizes and have different velocity and special profiles. In the femtosecond regime the laser-material interaction is far more efficient owing to the fact that there is insufficient time for electron-phonon coupling to occur within the time scale of the laser pulse. This means that the electronic system of the material reaches high temperatures and the lattice is relatively cold at the end of the pulse. This steep temperature gradient leads to the efficient transfer of thermal energy from the electronic system to the lattice and thus the volume of heated material is confined by the laser beam diameter and the optical penetration depth of the material. The optical penetration depth for Al, Ni and Au at 355 nm laser wavelength is 6.5, 13.0 and 15.0 nm, respectively [10]. This suggests that during fentosecond laser ablation at low fluence that the smaller more evenly heated volume of material results in the ejection of much smaller and a narrower distribution of nanoparticles than seen in the nanosecond regime.

The ambient environment was also investigated with a view to determining the influence of LIL on the generation of nanoparticles. For all three metals, the size of the nanoparticles were reduced when formed in $C_2H_2F_4$ relative to air. The generation of a liquid during laser ablation acts as an effective heat sink to disperse the thermal energy from the nanoparticles, thereby shortening their effective growth period and resulting in smaller nanoparticles.

The effect of $C_2H_2F_4$ was greatest on the Al nanoparticles, which resulted in a reduction in nanoparticle radius from 38.6 nm to 12.7 nm relative to those produced in air. The standard deviation was also reduced by more than half from 29.0 to 12.3 nm. The mean particle radius and standard deviation of Ni particles produced in the two ambients were similar, however the distribution in sizes showed that there was a greater tendency towards the mean particle size (35.0 nm). The distributions also showed that there are far fewer particles in excess of 200 nm produced in $C_2H_2F_4$ than in air. Au is of particular interest in that the maximum particle radius in $C_2H_2F_4$ was 17.5 nm and a standard deviation of 2.4 nm, whereas the spread was far larger in air with a maximum particle radius of 218.9 nm and a standard deviation of 19.8 nm. However, an observation of both Ni and Au distributions identified that there was a possible clustering effect in $C_2H_2F_4$ as the smallest nanoparticles seen in air were not present in $C_2H_2F_4$.

The reduction in nanoparticle size is as a result of the superior thermal conductivity of $C_2H_2F_4$ relative to air, which allowed for the efficient heat transfer from the plume. The formation of a liquid also increased the viscosity of the environment relative to air, which slowed the diffusion of particles, thereby reducing the number of particle-particle collisions and subsequent coagulation. This data therefore supports the premise that LIL can be applied during laser generation of nanoparticles to gain more control over the process and produce more controlled distributions of nanoparticles.

5. Conclusions

The interaction between laser pulses and a metal target is complex due to the dynamic nature of the ablation environment and consequently it is difficult to characterize the process of nanoparticle formation and growth. The objective to control this nanoparticle evolution is a non-trivial matter and requires a great deal more insight into the mechanisms involved. The biggest impact on the nanoparticle size and distribution came from the pulse duration, but the introduction of LIL was certainly of great influence and should be considered for optimizing the process.

Femtosecond laser ablation of metals resulted in substantially smaller nanoparticles for all three metals than during nanosecond laser ablation e.g. Al nanoparticles reduced from 36.8 nm in radius to 9.1 nm, respectively. The metal also influenced the resultant nanoparticles, for example gold characteristically produced very small nanoparticles (<10 nm) under all conditions, whereas nickel typically agglomerate to form larger aggregate structures.

The ambient environment was also very important and the process of LIL was shown to have a positive effect on narrowing the size distribution of nanoparticles. E.g. Al nanoparticles reduced from 36.8 nm in radius to 12.7 nm in $C_2H_2F_4$ relative to air. However, for Ni and Au nanoparticles there may be evidence of clustering of some of the smallest nanoparticles. In conclusion, to generate the smallest nanoparticles with the narrowest size distribution, a number of factors must be considered including laser pulse duration and beam shapes, metals with high electron-phonon coupling constants and thermal conductivity and ambient environments with high thermal conductivity.

Acknowledgements

This work was conducted under the framework of the INSPIRE programme, funded by the Irish Government's Programme for Research in Third Level Institutions, Cycle 4, National Development Plan 2007-2013. This work was sup- ported by Enterprise Ireland: CFTD/2004/316. This work was also supported by an EU Marie Curie Early Stage Training grant (MEST-CT-2005-020353) and with IRCSET funding. This work was also facilitated by The Atomic Microscopy Laboratory at CRANN in TCD.

References

[1] Gouriet, K.; Zhigilei, L.V.; Itina, T.E.: Molecular dynamics study of nanoparticle evolution in a background gas under laser ablation conditions. Applied Surface Science, 2009. 255(10): p. 5116-5119.
[2] Ausanio, G.; et al.: Production of nanoparticles of different materials by means of ultrashort laser pulses. Applied Surface Science, 2006. 252(13): p. 4678-4684.
[3] Haustrup, N.; Sedao, X.; Conneely, A.; O'Connor, G.M.: Laser-Induced Liquefaction of Tetrafluoroethane and Sulfur Hexafluoride Gases. The Journal of Physical Chemistry C, 2011: DOI 10.1021/jp108855
[4] Amoruso, S.; Toftmann, B.; Schou, J.: Broadening and attenuation of UV laser ablation plumes in background gases. Applied Surface Science, 2005. 248(1-4): p. 323-328.
[5] Zhu, X.P.; et al.: Underwater laser ablation approach to fabricating monodisperse metallic nanoparticles. Chemical Physics Letters, 2006. 427(1-3): p. 127-131.
[6] Vafaei, S; Wen, D.: Bubble formation in a quiescent pool of gold nanoparticle suspension. Advances in Colloid and Interface Science, 2010. 159(1): p. 72-93.
[7] Zhang, J.M.; et.al.: Calculation of the surface energy of fcc metals with modified embedded atom method. Applied Surface Science, 2004. 229(1-4): p. 34-42.
[8] Lin, Z.: Electron-Phonon and Electron Heat Capacity of Metals Under Conditions of Strong Electron-Phonon Non-Equilibrium. Physical Review B, 2008. 77.
[9] Hale, P.S.; et al.: Growth Kinetics and Modeling of ZnO Nanoparticles. Journal of Chemical Education, 2005. 82(5): p. 775-null.
[10]Palik, E.D.: Handbook of Optical Constants of Solids. Academic Press Handbook Series. 1985: Harcourt Brace Jovanovich Publishers.